Journal of *Marine Science and Engineering*

MDPI

*Article*

# Response of Foraminifera to Anthropogenic Nicotine Pollution of Cigarette Butts: An Experimental Approach

**Anna Sabbatini [1,*], Francesca Caridi [1], Giovanni Birarda [2], Elisa Costanzi [1,3], Adolfo Amici [3], Giovanna Mobbili [1], Carla Buosi [4], Giovanni De Giudici [4], Daniela Medas [4] and Alessandra Negri [1]**

1 Dipartimento di Scienze della Vita e dell'Ambiente, DISVA, Università Politecnica delle Marche, 60131 Ancona, Italy; f.caridi@univpm.it (F.C.); elisa.costanzi@iusspavia.it (E.C.); g.mobbili@univpm.it (G.M.); a.negri@univpm.it (A.N.)
2 Elettra—Sincrotrone Trieste S.C.p.A., SS 14, Km 163,5, Basovizza, 34149 Trieste, Italy; giovanni.birarda@elettra.eu
3 Dipartimento di Scienze Cliniche, Specialistiche e Odontostomatologiche, DISCO, Università Politecnica delle Marche, 60131 Ancona, Italy; a.amici@univpm.it
4 Dipartimento di Scienze Chimiche e Geologiche, Cittadella Universitaria, S.S. 554 Bivio per Sestu, Monserrato, 09042 Cagliari, Italy; carla.buosi@unica.it (C.B.); gbgiudic@unica.it (G.D.G.); dmedas@unica.it (D.M.)
* Correspondence: a.sabbatini@univpm.it

**Abstract:** The most often dispersed environmental pollutants that are released both directly and indirectly into the environment that may eventually reach aquatic ecosystems and contaminate aquatic biomes are cigarette butts (CBs). Toxicants such as nicotine, dangerous metals, total particulate matter, and recognized carcinogens can be introduced and transported via CBs into aquatic ecosystems. The examination of the effects of synthetic nicotine on three different species of cultured benthic foraminifera was the focus of this study. Three foraminiferal species from three distinct biomineralization pathways were specifically examined for viability and cellular ultrastructure, including the calcareous perforate *Rosalina globularis*, the calcareous imperforate *Quinqueloculina* spp., and the agglutinated *Textularia agglutinans*. The survival rate, cellular stress, and decalcification were used to assess the toxicological effects of synthetic nicotine. We were able to analyze the reaction of major macromolecules and calcium carbonate to this pollutant using FTIR (Fourier Transform Infrared) spectroscopy. High Performance Liquid Chromatography (HPLC) study was performed to increase our understanding of nicotine bioavailability in the medium culture. Different acute experiments were performed at different dates, and all indicated that synthetic nicotine is acutely hazardous to all three cultured foraminiferal taxa at lethal and sublethal concentrations. Each species responded differently depending on the type of shell biomineralization. Synthetic nicotine enhances shell decalcification and affects the composition of cytoplasmic macromolecules such as lipids and proteins, according to the FTIR spectroscopy investigations. The lipid content rose at lethal concentrations, possibly due to the creation of vesicles. The proteins signal evidences general cellular dyshomeostasis. The integration among the acute toxicity assay, synchrotron, and chemical HPLC analyses provided a valuable approach for the assessment of nicotine as a biomarker of exposure to the toxicants associated with smoking and the impact of this emerging and hazardous material on calcifying marine species.

**Keywords:** nicotine; CBs; foraminifera; anthropogenic pollutants; marine litter; decalcification



**Citation:** Sabbatini, A.; Caridi, F.; Birarda, G.; Costanzi, E.; Amici, A.; Mobbili, G.; Buosi, C.; De Giudici, G.; Medas, D.; Negri, A. Response of Foraminifera to Anthropogenic Nicotine Pollution of Cigarette Butts: An Experimental Approach. *J. Mar. Sci. Eng.* **2023**, *11*, 1951. https://doi.org/10.3390/jmse11101951

Academic Editor: Petra Heinz

Received: 16 August 2023
Revised: 29 September 2023
Accepted: 2 October 2023
Published: 10 October 2023



## 1. Introduction

Marine debris is a worldwide environmental issue. Chemical dispersal affects the chemistry of water and sediments, hence affecting the environmental quality and, eventually, the trophic chain [1]. Several studies have found that smoked cigarette butts (CBs) form a significant component of marine litter in the Mediterranean coasts [2], in South America [3], and in Australia [4]. CBs are the most common type of human-made coastal

litter that can bioaccumulate in marine organisms [5,6]. Toxins such as nicotine, hazardous metals, total particulate matter, and recognized carcinogens can be transported and introduced into aquatic environments via CBs [7].

While the health hazards associated with cigarette smoking have been addressed for decades ([8]; USDHHS 2014), the fate of CBs after disposal has only lately received some consideration (reviewed by [5,9]). CBs, in particular, were categorized as hazardous waste by European regulations due to their acute toxicity (H6), mostly due to the nicotine concentration [10]. Indeed, the distribution and diffusion of CBs and their associated toxicants in the aquatic environment can pose a threat to a variety of prokaryotic and eukaryotic species that live in these settings [9].

Nonetheless, current knowledge on the hazards and toxicological effects of CBs in marine organisms is still patchy, depending on the different experimental conditions considered, namely the effects of direct exposure to CBs' leachates on species survival, growth, or reproduction, and the fate and effects of CBs on the environment. Few studies focused on marine organisms after [9]; for example, *Alivibrio fischeri* (bacteria) loses its bioluminescence [11,12] and the microbial community in coastal marine sediments changes [13]. Despite a drop in chlorophyll concentration in the mesocosm, the macroalga *Ulva lactuca* appears unaffected by CBs pollution [14]. Microalgae *Phaeodactylum tricornutum*, *Skeletonema costatum*, and *Dunaliella tertiolecta* have a distinct reaction, with growth inhibition [12]. The snails *Austrocochlea porcata, Nerita atramentosa,* and *Bembicium nanum* exhibit behavioral changes [15], but the ragworm *Hediste diversicolor* loses its borrowing capacity, slows down growth, and increases DNA damage [16]. When exposed to CBs, the filter feeder *Mytilus edulis* (blue mussel) reduces its clearance rates thrice compared to unpolluted mesocoms [14]. Ex vivo research on thin sections of *Mytilus galloprovincialis* digestive glands reveals an overall decrease in the genetic transcription levels for exposed tissues [12]. If nicotine is bioavailable, the in vivo exposure of mussels to CBs results in tissue damage as well as a considerable deterioration of indicators of immunological, genotoxic, and neurotoxic damage [12]. The presence of deformed larvae inhibits larval development in another bivalve, *Crassostrea gigas* [12]. Finally, CBs are toxic to the marine topsmelt *Atherinops affinis* and the fish *Periophthalmus waltoni* [17].

These studies clearly show the influence of CBs on marine species; however, none of them look at the impact of CBs and its associated toxicants on shells and the potential negative effects on biocalcification processes. Ref. [18] exhibited cellular mortality of unicellular eukaryotic foraminifera as well as the decalcification of their calcitic tests during an acute toxicity experiment (LC50 48 h) cultured in CBs' leachate. These authors demonstrated, using FTIR (Fourier-transform infrared) spectroscopy, that foraminiferal death and decalcification could be caused by a combination of pH reduction caused by CBs leachate and the toxicity of other dissolved substances, particularly nicotine (32 CB/L stock solution corresponding to 62.5 mg of nicotine/L), which leads to physiology alteration and, in many cases, cellular death.

Nicotine is neurotoxic, affecting the central and autonomic nervous systems, as well as neuromuscular junctions, by agonistically binding to nicotinic acetyl cholinergic receptors (nAChRs) [19]. This opens ion channels, allowing sodium or calcium ions to enter and increase the neurotransmitter release. Although foraminifera are unicellular organisms, they have ion channels (i.e., calcium) in their cellular membrane that aid in the biomineralization process. Ref. [20] revealed that two calcareous perforate foraminiferal species were particularly sensitive to a calcium channel blocker, indicating that trans-membrane transport carries the majority of calcium ions required during calcification.

For these reasons, we want to extend these preliminary findings with an acute toxicity experiment (LC50 48 h) using only a synthetic nicotine leachate to investigate the possible impact of this single parameter.

The viability and ultrastructure of three foraminiferal species from three different biomineralization pathways are examined in this study: the calcareous perforate *Rosalina globularis*, the calcareous imperforate *Quinqueloculina* spp., and the agglutinated *Textu-*

*laria agglutinans*. The toxicological effects of synthetic nicotine on survival rate, cellular stress, and decalcification were studied. We were able to analyze the response of major macromolecules and calcium carbonate to this pollutant using FTIR spectroscopy. High Performance Liquid Chromatography (HPLC) study was performed to increase our understanding of nicotine bioavailability in the medium culture.

The combination of acute toxicity assays, synchrotron, and chemical HPLC investigations provides a valuable strategy for evaluating nicotine as a biomarker of exposure to toxicants associated with smoking, as well as the influence of this hazardous substance on calcifying marine species.

## 2. Materials and Methods

### 2.1. Foraminiferal Species

This study focused on three benthic foraminiferal species: *Rosalina globularis*, *Textularia agglutinans*, and *Quinqueloculina* spp. The specimens have grown in the isolated monospecific cultures maintained at the DISVA (UNIVPM) Laboratory of Paleoecology. Ref. [18] was followed for foraminiferal culture maintenance. The selection of these three taxa relies on their distinct shell structure and ecology. *Rosalina globularis* is a widespread symbiotic foraminiferal species used as a model in ecotoxicological investigations [18,21], while *Quinqueloculina* and *Textularia* are shallow-water genera present near anthropized coastlines [22]. For specific information on the shell structures and composition of these three taxa, we refer the interested readers to [21], where comprehensive details can be found. Furthermore, the benthic foraminiferal species used in this study were the same as those used by [18] for the acute toxicity test. We chose individuals ranging in size from 90 to 150 mm for the experiment in order to obtain adult specimens rather than juvenile forms, which could bias taxonomy identification. Then, using a fine brush, living species were collected for the experiment, and their vitality was validated by examining their behaviors (i.e., food gathering, pseudopodial activity) under the optical microscope.

### 2.2. Experimental Design

The experiments which were conducted in December 2020 and April 2021 were based on the acute exposure (48 h) of the chosen foraminiferal species to a synthetic nicotine solution at sublethal and lethal concentrations using the [18] protocol.

On the benthic cultured foraminifera, the acute toxicity of human-smoked CBs leachate was evaluated (LC50 48 h). The CBs leachate contains primarily nicotine (62.5 mg/L), according to the gas chromatography-mass spectrometry (GC-MS) study of the CBs stock solution [18]. We calculated the corresponding quantity of synthetic nicotine (mg/L) for each target foraminiferal species employed in the current study using the sublethal and lethal amounts of CBs leachate reported by [18] (Table 1).

**Table 1.** Volume of synthetic nicotine (mg/L) derived from the sublethal and lethal concentrations of CBs' leachate obtained by [18] for each target species.

| Species | *Rosalina globularis* | *Quinqueloculina* spp. | *Textularia agglutinans* | References |
|---|---|---|---|---|
| **CTRL** | 0 | 0 | 0 | |
| **SUBLETHAL** | | | | |
| CBs (mg/L) | 1 | 2 | 2 | [18] |
| Synthetic Nicotine (mg/L) | 1.96 | 3.91 | 3.91 | Current study |
| **LC50** | | | | |
| CBs (mg/L) | 1.9 | 7.2 | 5.6 | [18] |
| Synthetic Nicotine (mg/L) | 3.72 | 14.11 | 10.98 | Current study |

To obtain a synthetic nicotine concentration of 35 g/L, the stock solution was made by mixing 10 mL of a 35% synthetic nicotine solution (Nicotine hemisulfate salt, Sigma Aldrich, St. Louis, MO, USA) with 90 mL of artificial seawater. After being stabilized overnight, the artificial saltwater produced by mixing 2 L of deionized water with 75 g of Instant Ocean® had a pH range of 8.0 to 8.4 and a salinity range of 35 to 37 psu.

Two acute 48 h toxicological experiments were performed in December 2020 and April 2021; for all three foraminiferal taxa, three replicates for both the lethal and sublethal concentrations of synthetic nicotine were taken, plus one control.

For December 2020, each replicate contained five individuals, yielding 35 individuals for each species and synthetic nicotine concentration. Due to the limited number of *T. agglutinans* individuals observed during the picking phase, all *T. agglutinans* replicates in April 2021, however, comprised only three individuals. The experiments were conducted under laboratory conditions, and the pH, salinity, and temperature readings of the water quality of each jar were taken before and after the experiment.

Following the experimental treatments, a survival count using [23] was carried out. All foraminiferal specimens were taken and removed from the jars using a brush, and all traces of the nicotine stock solution were washed away by rinsing them three times in clean seawater. After that, they were incubated for 30 min in Petri dishes containing 15 mL of filtered seawater and 0.4 L of the fluorescent probe Cell Tracker Green (CTG) that is a vital fluorogenic probe developed to exclusively stain living cells [24]. Following this, the foraminifera were once more rinsed in clean saltwater to eliminate any remaining CTG before being examined using a fluorescence binocular microscope to look for signs of cellular activity.

Following the protocols set by [25], the foraminiferal specimens were then maintained for 72 h in clean seawater, and the color and activity of each individual were visually inspected to detect potential quiescent organisms (recovery phase). Dead individuals have to be distinguished from survivors during the recovery phase in order to remove them from the count.

### 2.3. High Performance Liquid Chromatography Analysis (HPLC)

The Polytechnic University of Marche's Department of Specialist Clinical and Odontostomatological Sciences (DISCO) performed the HPLC analysis in the A2021 acute toxicity test. This analysis was performed to check for the presence of synthetic nicotine and its primary metabolite, cotinine, in the culture medium in which the foraminifera were cultured (hereinafter N%: synthetic nicotine recovery rate). The extraction technique was developed with some modifications to the [26], 2009 methodology. A Young Lin Instruments chromatograph was used, consisting of a YL9111 binary pump, a YL9160 PDA detector, and an HTA-MT300L-E auto-sampler (HTA s.r.l., Brescia, Italy) operated via its integrated software and connected to a C-18 reverse phase column, Synergi RP 4 µm, 80 A, 250 mm × 4.6 mm i.d. (Phenomenex Inc., Torrance, CA, USA). The column was equilibrated with 0.050 M of $KH_2PO_4$ buffer, adjusted to pH 6.1 via KOH, containing 5 mM of Heptane-1-Sulfonic Acid sodium salt as the ion pair agent, at a 1.0 mL/min flow rate (buffer A), and washed with 40% methanol in the same buffer (buffer B) in between samples. Chromatograms were acquired using a diode array detector and integrated at a 260 nm wavelength using the nicotine and cotinine standards for quantization. Compounds were identified using the retention time and UV spectrum correspondence. Quality assurance and quality control for the HPLC analyses were checked by processing the reference standard materials (cotinine, nicotine salt, and pure nicotine, all from Sigma-Aldrich, St. Louis, MO, USA) and the blank samples. The concentrations obtained from these reference standard materials were consistently confined within the certified values' 95% confidence ranges.

Details on the analytical methods and procedures are given in Appendix A.

### 2.4. Fourier Transform Infrared Analyses

The Fourier Transform Infrared (FTIR) analysis was performed on April 2021 with SISSI beamline, the biochemical and life sciences branch (SISSI-Bio) at Elettra Sincrotrone Trieste [4], to assess the cell damage and estimate the potential calcium carbonate loss that the three foraminiferal genera may have undergone. The foraminiferal samples were measured, and the samples were inspected under a Zeiss Stemi 305 optical microscope, and then transferred onto the Diamond compression cell (S.T. Japan-Europe GmbH, Cologne, Germany). There, the two halves of the cell were placed on the top of the other and the samples were slowly compressed between the two diamonds. Once the sample was pulverized and compressed enough to be measured in transmission mode, the cell was opened and put under the Hyperion 3000 optical/infrared microscope (Bruker Optics, Billerica, MA, USA). For each sample, the whole imprint left on the face of the compression cell was measured in transmission mode with a 64 × 64-pixel Focal Plane Array (FPA), collecting 128 scans at a 4 $cm^{-1}$ spectral resolution. The pixel size acquired with 15× IR/VIS objective/condenser Cassegrain optics is 2.66 × 2.66 µm. For the smaller samples, imaging before closing the cell was performed with the same acquisition parameters described before.

To evaluate the nicotine effect on foraminifera, band integrals were calculated: 1700–1605 $cm^{-1}$ for proteins (Amide I), representative of the cytoplasm; 3000–2800 $cm^{-1}$ for lipids; 2660–2435 $cm^{-1}$ overtone; 1850–1765 $cm^{-1}$ for calcium carbonate; and 1200–950 $cm^{-1}$ for phosphates, silicates, and carbohydrates. The results of the band's integration were calculated in Quasar (https://quasar.codes, accessed on 1 January 2023), and the outlier values were removed and then averaged for every treatment in order to allow for comparison. Integrals were analyzed with one-way ANOVA and plotted in Origin (Origin, OriginLab Corporation, Northampton, MA, USA). Average spectra were calculated in Quasar, and two PCAs were performed after filtering out the spectra corresponding to the empty areas with a k-means clustering: one on the vector normalized data over the complete spectral range and the second on the vector normalized 2nd derivative Amide I (1700–1605 $cm^{-1}$). Origin (Origin labs) was used to plot the results of the PCAs.

## 3. Results

### 3.1. Foraminiferal Acute 48 h Toxicological Tests

During both the acute 48 h toxicological experiments of December 2020 and April 2021, the measure of the seawater quality parameters (T, S and pH) showed minimal changes from 22 to 22.6 °C for temperature, 35 to 36 psu for salinity, and 8.23 to 8.36 for pH, which are not relevant if compared to the pre-test conditions. Figure 1a shows the concentration–response curve of the December 2020 acute experiment, evidencing that as the concentration of synthetic nicotine in the samples increased, the percentage of alive foraminifera decreased linearly for *Quinqueloculina* spp., while for the other two species (*R. globularis* and *T. agglutinans*), after a significant initial reduction, it tended to stabilize, reaching 20% at the lethal concentration. The same figure shows that instead, a linear relationship between the concentration of synthetic nicotine and the foraminiferal survival rate characterized the results of the April 2021 acute experiment. Here, the percentage of living individuals decreased as the concentration of synthetic nicotine increased. At the lethal concentration, *T. agglutinans* reached zero (Figure 1b). Figure 1c presents the mean values of all samples from *R. globularis*, *Quinqueloculina* spp., and *T. agglutinans* (control, sublethal, and LC50) for the acute tests conducted on December 2020 and April 2021. The outcomes depicted in Figure 1c underscore that the foraminiferal species subjected to incubation in the samples of the control, sublethal, and lethal nicotine solutions exhibited distinct behaviors that were statistically significant. This finding confirms that *Quinqueloculina* spp. stands out as the most resistant taxonomic group among them. On the contrary, Rosalina globularis and *Textularia agglutinans* exhibited distinct sensitivities in the two acute tests. In particular, *T. agglutinans* displayed extreme vulnerability to lethal synthetic nicotine pollution in April 2021, while in December, both *T. agglutinans* and *Quinqueloculina* spp. exhibited a similar declining trend in response to the lethal nicotine solution.

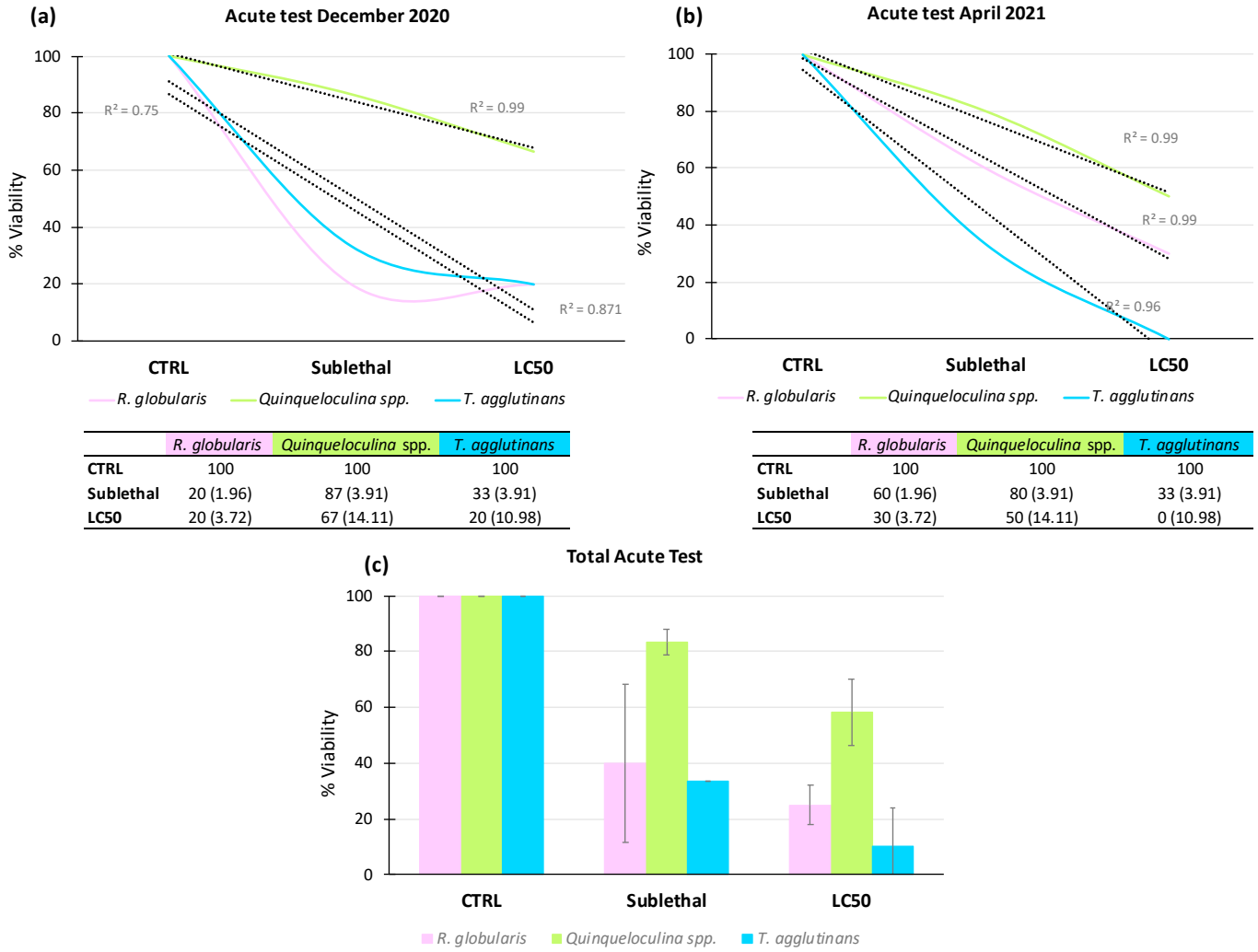


| | *R. globularis* | *Quinqueloculina* spp. | *T. agglutinans* |
|---|---|---|---|
| **CTRL** | 100 | 100 | 100 |
| **Sublethal** | 20 (1.96) | 87 (3.91) | 33 (3.91) |
| **LC50** | 20 (3.72) | 67 (14.11) | 20 (10.98) |

| | *R. globularis* | *Quinqueloculina* spp. | *T. agglutinans* |
|---|---|---|---|
| **CTRL** | 100 | 100 | 100 |
| **Sublethal** | 60 (1.96) | 80 (3.91) | 33 (3.91) |
| **LC50** | 30 (3.72) | 50 (14.11) | 0 (10.98) |

**Figure 1.** (**a**) Synthetic nicotine concentrations vs. percentage of survived foraminifera (December 2020 acute 48 h toxicological test) for the three studied species: *Rosalina globularis* (pink), *Quinqueloculina* spp. (green), and Textularia agglutinans (light blue). (**b**) Synthetic nicotine concentrations vs. percentage of survived foraminifera (April 2021 acute 48 h toxicological test). Tables show the percentage of viability from both acute toxicological tests and all target foraminiferal species. Values in brackets indicate the synthetic nicotine concentration corresponding to sublethal and lethal levels for each taxon. Dotted lines represent the linear regression with values of $R^2$. (**c**) Synthetic nicotine concentrations vs. percentage of survived foraminifera for both acute tests.

### *3.2. High Performance Liquid Chromatography*

The HPLC data only refer to the April 2021 48 h acute toxicological test. Except for the control samples, the chromatograms of all nicotine-solution samples revealed a fairly similar pattern for synthetic nicotine, with a maximal absorption peak around 15 min confirming its existence in the solutions. No cotinine peak was found in any of the samples. Appendix B shows the synthetic nicotine recovery rates (N%) for each nicotine-solution sample incubated with the target foraminiferal species. Almost all values (Table 2; Figure 2) were less than 20%. Since the toxicant was not present in the control-solution samples, the synthetic nicotine recovery rate was plainly 0%.

**Table 2.** Synthetic nicotine recovery rate values expressed in % and calculated on all culture medium samples in which target foraminiferal species were incubated. Medium values and standard deviation are shown.

| Foraminiferal Species | Replicates | Synthetic Nicotine Recovery Rate (%) | | |
|---|---|---|---|---|
| | | CTRL | Sublethal | LC50 |
| *Rosalina globularis* | R1 | 0 | 18.3 | 15.7 |
| | R2 | 0 | 31.8 | 13.7 |
| | R3 | 0 | 17.0 | 19.3 |
| Medium value | | | **22.36** | **16.23** |
| Standard deviation | | | **8.20** | **2.84** |
| | | CTRL | Sublethal | LC50 |
| *Quinqueloculina* spp. | R1 | 0 | 12.9 | 14.0 |
| | R2 | 0 | 13.6 | 15.6 |
| | R3 | 0 | 16.4 | 14.1 |
| Medium value | | | **14.3** | **14.5** |
| Standard deviation | | | **1.85** | **0.90** |
| | | CTRL | Sublethal | LC50 |
| *Textularia agglutinans* | R1 | 0 | 10.7 | 15.3 |
| | R2 | 0 | 15.9 | 14.1 |
| | R3 | 0 | 15.2 | 13.6 |
| Medium value | | | **13.93** | **14.33** |
| Standard deviation | | | **2.82** | **0.87** |

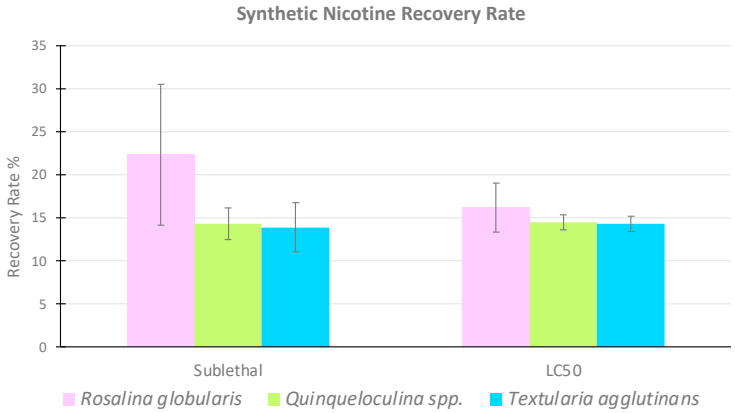


**Figure 2.** Synthetic nicotine recovery rate expressed in % in nicotine-solution used for the toxicological experiment. It is the percentage of the chemical present in the culture medium in which foraminifera were cultivated (N%).

The values of synthetic nicotine recovery rate were comparable for both the sublethal and lethal concentrations in the nicotine-solution samples where Textularia agglutinans and *Quinqueloculina* spp. were incubated. *T. agglutinans* values, in particular, varied from a minimum of 10.7% in the sublethal sample R1 to a maximum of 15.9% in the sublethal sample R2. From 12.9% (sublethal sample R1) to 16.4% (sublethal sample R3), *Quinqueloculina* spp. values changed. Rosalina globularis had the highest range of synthetic nicotine recovery rates, with values ranging from 13.7% in the LC50 sample R2 to 31.8% in the sublethal sample R2 (Table 2).

### *3.3. Fourier Transform Infrared (FTIR)*

The data obtained via the infrared spectroscopy analyses allowed us to assess the synthetic nicotine effects on the biochemical composition of foraminiferal cells and tests, focusing on biocalcification processes. Figure 3 displays the average spectra of all *Rosalina globularis* (Figure 3a), *Quinqueloculina* spp. (Figure 3b), and *Textularia agglutinans* (Figure 3c)

samples (control, sublethal and $LC_{50}$). In some cases, the band between 1500–1300 $cm^{-1}$ showed a signal too strong from carbonates, and therefore, it was not used for the estimation of carbonates in the samples. The *Quinqueloculina* spp. sublethal data are not shown because it was not possible to analyze any single individual. Figure 3c shows the sublethal and $LC_{50}$ spectra of the *T. agglutinans* samples that had a different trend, as can be observed from the different height of the blue peak (sublethal) and the red peak ($LC_{50}$) in the range of phosphates, silicates, and carbohydrates (1000–1200 $cm^{-1}$). This variation was neither observed in *R. globularis* (Figure 3a) nor in *Quinqueloculina* spp. (Figure 3b), but in these species, there was a difference between the control (black line) and the $LC_{50}$ samples' (red line) averaged spectra in the protein range corresponding to Amide I (1700–1605 $cm^{-1}$). The protein signal of the sublethal spectrum for *R. globularis* was less evident. The *Quinqueloculina* spp. $LC_{50}$ samples (red line) showed intense signals, but to evaluate the eventual decalcification of their carbonatic shells, we analyzed the band ratio. Therefore, Figure 3d shows the values of the ratios for the carbonates over the total amount of protein for the three target species, namely the index of the ratio between the mineral part and the organic one. The results in Figure 3d evidence that foraminiferal species incubated in the control, sublethal and lethal nicotine-solution samples had a statistically different behavior.

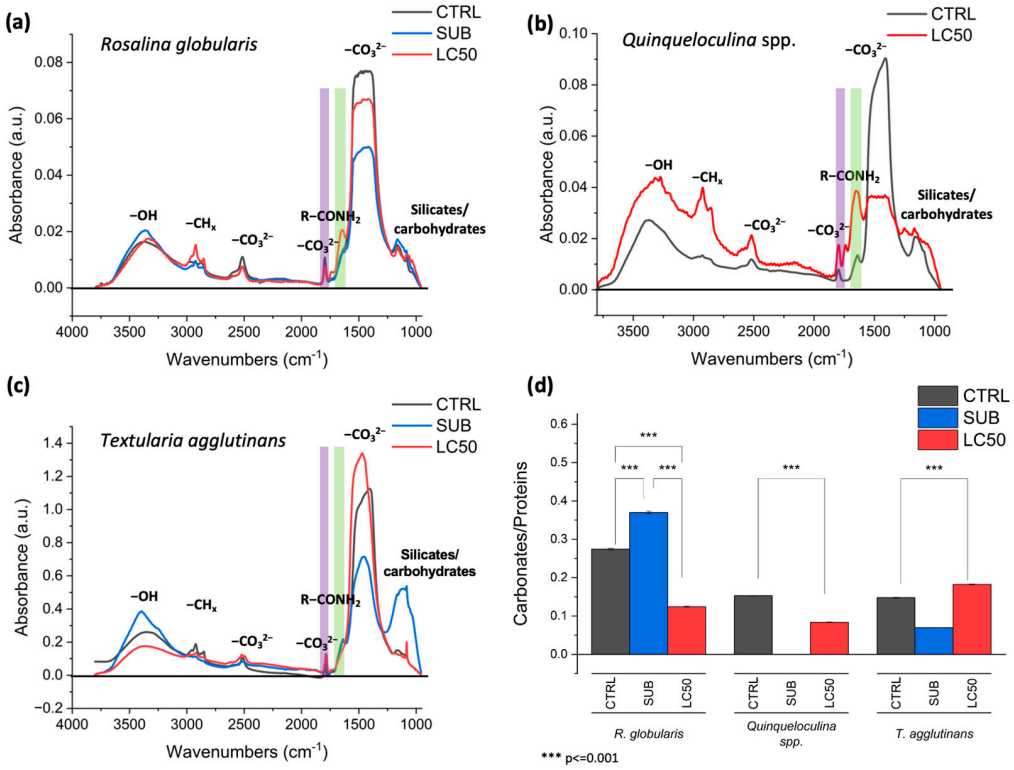


**Figure 3.** Average spectra of the three target species: (**a**) *Rosalina globularis*, (**b**) *Quinqueloculina* spp., and (**c**) *Textularia agglutinans*. In violet is highlighted the spectral range of the $CO_3^{2-}$, and in green is highlighted the spectral range of Amide I of proteins. The signals in these ranges are utilized for the calculation of the ratio shown in panel D. (**d**) The comparison of carbonate over protein averages for the three different species was shown for the two concentrations of synthetic nicotine (sublethal and lethal) in relation to the pristine situation (control). CTRL: control; SUB: sublethal; LC50: lethal.

Considering the sublethal concentration used to contaminate the culture medium in which foraminifera were incubated, *R. globularis* and *T. agglutinans* had an opposite trend compared with the control values. In particular, the carbonates/proteins ratio decreases in *T. agglutinans*, probably due to a small increase in the protein signal, and there is a contemporary significant increase in the silicates and carbohydrates band centered around 1100 $cm^{-1}$ (Figure 3c). There is also a strong decrease in the carbonate bands. Whereas for *R. globularis*, there is a temporary increase in the carbonates/proteins ratio (Figure 3d); this

trend, observing the spectra, could correspond to a decrease in the cellular protein content (Figure 3a, violet areas). Due to the technical problems, it was not possible to acquire any data at the sublethal concentration for *Quinqueloculina* spp.

The calcareous species *R. globularis* and *Quinqueloculina* spp. responded to the incubation with the lethal concentration by losing calcium carbonate, as shown by a decrease in the carbonates/proteins ratio compared to the control values (Figure 3d); additionally, they accumulated proteins and carbohydrates, as evidenced by the bands centered at 1700–1605 $cm^{-1}$ and 1100 $cm^{-1}$, respectively (Figure 3a,b). On the other hand, the carbonates/proteins ratio rose in the agglutinated species *T. agglutinans*, indicating a decrease in proteins relative to the calcium carbonate in the shell.

Then, the data were further analyzed using the principal component analysis (PCA). In this way, it was possible to detect subtler peak variations induced by the acute 48 h toxicological experiment using synthetic nicotine. The analyses were carried out twice: the first analyses were performed using the complete spectral range in absorbance, then for the second one, only the 2nd derivative of the Amide I (1700–1605 $cm^{-1}$ region) was considered when focusing, in particular, on the protein conformational variations induced by the treatments. The two PCAs for the perforate calcareous species *R. globularis* are shown in Figure 4. When taking into account the full spectral range, there is no obvious difference between the control, sublethal, and LC50 samples in *R. globularis*. The *R. globularis* samples that were incubated at sublethal concentrations (shown by the blue ellipse in Figure 4a) clustered with the control (black) and the majority of the LC50 (red) clusters rather than separately from the other samples. Part of the $LC_{50}$ measures separated from the controls and the sublethal concentration along the PC4 axis (Figure 4a). The spectral loading corresponding to PC4 is shown in Figure 4b; here, signals in the lipid regions at 2925 $cm^{-1}$, 2855 $cm^{-1}$, and 1735 $cm^{-1}$ hint at an increase in the lipid content.

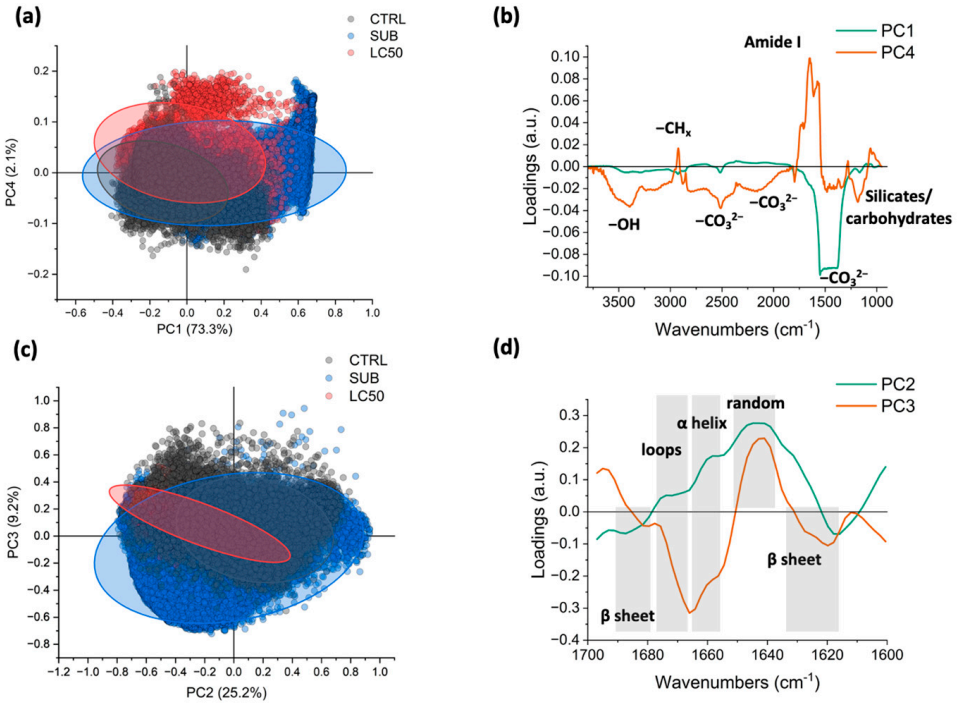


**Figure 4.** PCAs of *Rosalina globularis* species. (**a**) scatterplot and (**b**) loading vectors refer to the PCA of the complete spectral range of this species. In (**c**), the scatterplot result of the PCA analysis in the protein range is shown, and in (**d**), the corresponding loading vectors are shown with the main protein structures evidenced and identified in gray. CTRL: control; SUB: sublethal; LC50: lethal.

Regarding the protein conformation, the PCA does not show a clear separation between the three clusters (Figure 4c), even though the *R. globularis* samples incubated at the

sublethal and $LC_{50}$ concentrations lean towards the negative hemispace of PC2 more than the control samples; this is linked to an increase in the 1640 $cm^{-1}$ and 1665 $cm^{-1}$ signals, where the first is assigned to random protein coil conformation and the second to the beta sheet aggregates indicative of accumulating the misfolded forms of proteins (Figure 4d).

For the imperforate calcareous species of *Quinqueloculina* spp, only the data from the control and LC50 samples were available, and the PCA analysis showed that PC1 and PC2 positives occur in the upper right quadrant of the treated samples (Figure 5a).

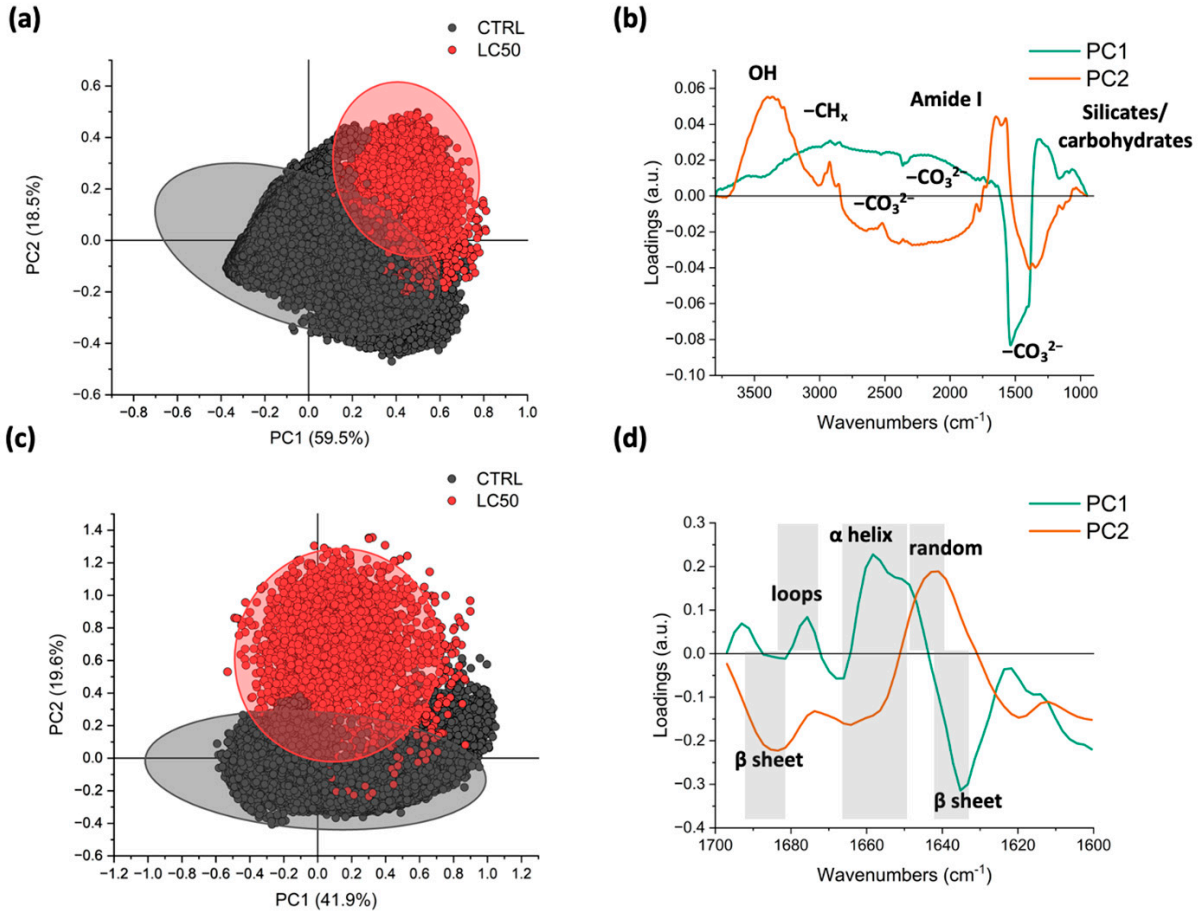


**Figure 5.** PCAs of *Quinqueloculina* spp. species. (**a**) scatterplot and (**b**) loading vectors refer to the PCA of the complete spectral range of this species. In (**c**), the scatterplot result of the PCA analysis in the protein range is shown, and in (**d**), the corresponding loading vectors are shown with the main protein structures evidenced and identified in gray. CTRL: control; SUB: sublethal; LC50: lethal.

Analyzing the loadings in Figure 5b, it is evident that PC1 is related mainly to the content of calcium carbonate since it shows all its main bands (2660–2435 $cm^{-1}$ and 1850–1765 overtones, and 1500–1300 $cm^{-1}$ broad band) that are higher in the control samples (left side of the scatterplot) and lower in most of the $LC_{50}$ spectra, whereas PC2 (Figure 5b) shows signals related to the lipids (3000–2800 $cm^{-1}$) and proteins (Amide I centered at 1640 $cm^{-1}$). Considering the analysis on the proteins' region only, the separation is stronger, and it is mainly on PC2, characterized by three negative peaks at 1685, 1665, and 1620 $cm^{-1}$, all of which can be associated to the beta sheets and aggregate structures that are more present in the *Quinqueloculina* spp. samples incubated in synthetic nicotine. Finally, Figure 6 shows the two scatterplots and two lines plots relative to the PCAs results of the agglutinated species *Textularia agglutinans*.

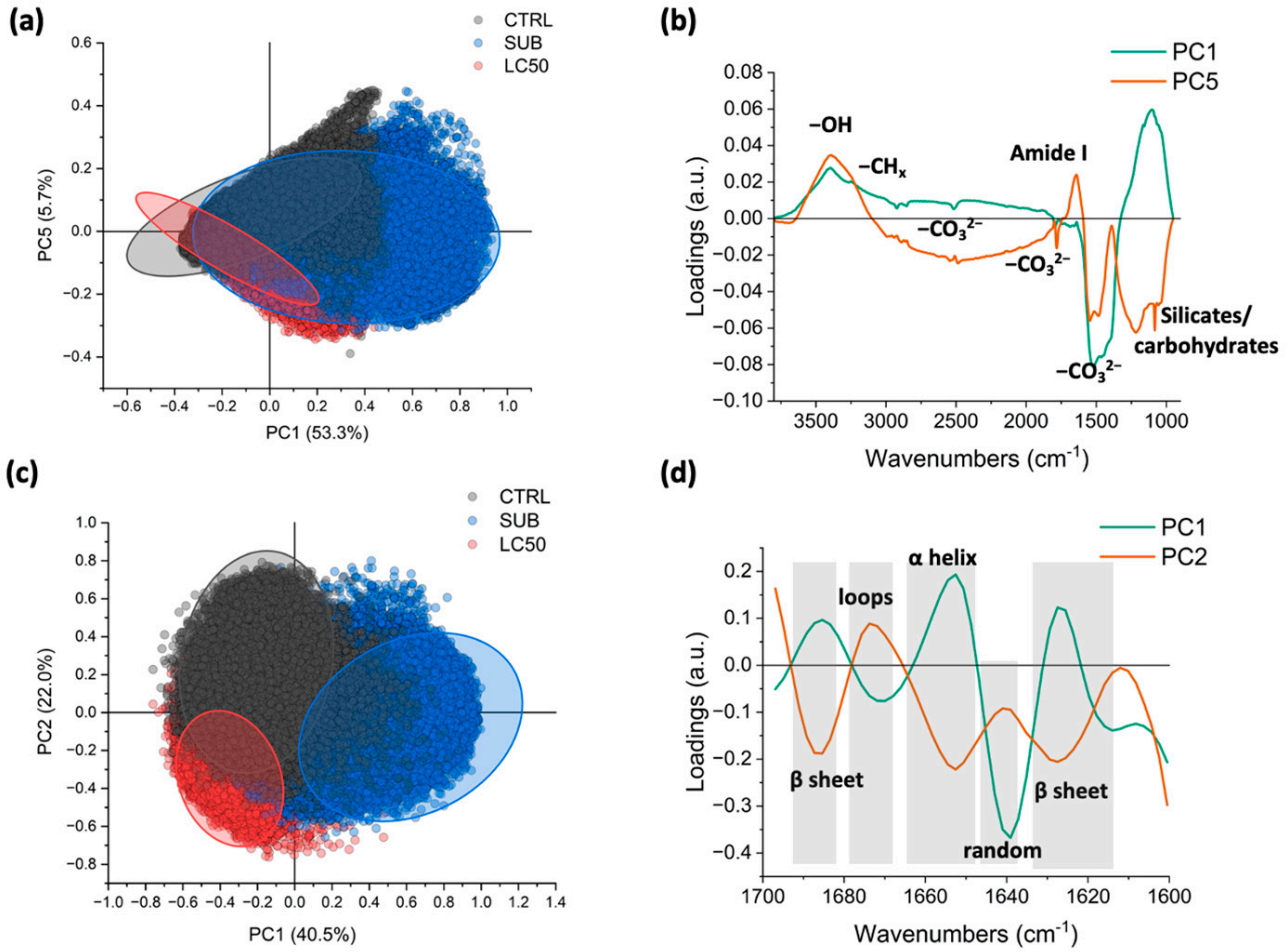


**Figure 6.** PCAs of *Textularia agglutinans*. species. Graphics' (**a**) scatterplot, and (**b**) loading vectors refer to the PCA of the complete spectral range of this species. In (**c**), the scatterplot result of the PCA analysis in the protein range is shown, and in (**d**), the corresponding loading vectors are shown with the main protein structures identified and evidenced in gray. CTRL: control; SUB: sublethal; LC50: lethal.

Some trends are evident, although there is a partial overlap of the *T. agglutinans* samples incubated in the sublethal and lethal concentrations and the control. The sublethal samples cluster is separated from the control and the $LC_{50}$ clusters along PC1 (positive hemiplane), whereas the part of the $LC_{50}$ and sublethal clusters are localized in the negative hemiplane for PC5 (Figure 6a). By analyzing the loading vectors aside, it is possible to see that PC1 had a positive broad band in the silicates and carbohydrates' spectral range (1300–1000 $cm^{-1}$) (Figure 6b). The scatterplot in panel 6c and 6d is focused on *T. agglutinans* protein trends. The control cluster is mainly in the positive hemiplane of PC2, and the sublethal and $LC_{50}$ clusters are in the negative one, where these two clusters are separated from each other along PC1 (Figure 6c). From the loadings, the PC1 has a strong peak at 1640 $cm^{-1}$ linked to the random coil conformation of proteins (Amide I), indicating disorder in the secondary structure of proteins of the *T. agglutinans* specimens incubated in the sublethal synthetic nicotine concentration. Instead, considering PC1, the proteins of *T. agglutinans* specimens intoxicated with the lethal nicotine-solution have a similar conformation of the control samples, but an overall lower intensity of the 2nd derivative, confirming the loss of proteins as a response to the treatments.

## 4. Discussion

### 4.1. Nicotine and Its Effect on the Foraminiferal Vitality

Nicotine (originally used as an herbicide) is probably the most highly researched chemical constituent of CBs, and it is the one that has raised the most public awareness. Moreover, nicotine is the principal alkaloid naturally present in tobacco leaves and it was the most abundant chemical compound released in leachates. Following the preliminary results obtained by [18], the aim of this research was to evaluate the impact of synthetic nicotine on three different taxa of cultured benthic foraminifera (*Rosalina*, *Quinqueloculina*, and *Textularia*). Ref. [18] reported the acute toxicity (LC50 48 h) of leachate from CBs that were smoked by humans. The study exposed the same foraminiferal taxa mentioned earlier to varying concentrations of CBs' leachate, specifically 16, 8, 4, 2, and 1 CB per liter (CB/L). These concentrations were obtained via the dilution of a stock solution prepared at 32 CB/L, which corresponded to a nicotine concentration of 62.5 mg per liter. Starting from 4 CB/L (approximately containing 8 mg of nicotine/L), two calcareous genera (*Rosalina* and *Quinqueloculina*) exhibited shell decalcification and death of almost all individuals, except for the more resistant agglutinated species (*Textularia agglutinans*). In addition, via the FTIR (Fourier-transform infrared) spectroscopy analysis, [18] it demonstrated that foraminiferal death and decalcification could be a result of pH reduction due to CBs leachate and the toxicity of other dissolved substances, particularly nicotine, which leads to physiological alterations and, in many cases, cellular death [18].

The present study further investigates these initial significant results with an acute toxicity assay using a synthetic nicotine solution to assess the potential effects of this single parameter.

The two acute tests (LC50 48 h) of December 2020 and April 2021 confirmed that synthetic nicotine is acutely toxic at lethal and sublethal concentrations for all three cultured foraminiferal taxa. Specifically, the viability values (Figure 1) showed that *Quinqueloculina* spp. was the most resistant taxon in both bioassays, while *R. globularis* and *T. agglutinans* were the most sensitive species in the December 2020 and April 2021 bioassays, respectively. Differences between the two acute tests could be attributed to various factors, including normal experimental variability and the distinct responses of individual specimens. We cannot exclude that factors like the metabolic and physiological status of the specimens, which may not be identifiable initially, can influence the foraminiferal responses to the experimental conditions. It is, however, worth noting that biomineralization in foraminifera primarily relies on the vital effect, wherein the production of calcium carbonate is intricately linked to the biological control within the cell, as so influenced by the organism's metabolic and physiological state. In any case, it was evident that different species, based on their biomineralization mechanisms, were sensitive to synthetic nicotine pollution. Indeed, all three taxonomic groups exhibited a clear mortality rate, with *T. agglutinans* showing a 100% mortality rate in the April 2021 experiment. This was observed when the specimens were cultured in a lethal concentration of synthetic nicotine, which corresponded to 10.98 mg/L of nicotine, equivalent to the discharge from 5.6 CB/L. Similar results were reported by [18], who observed 100% mortality for *R. globularis* exposed to CBs' leachate. Additionally, according to [12], different marine organisms exhibited species-specific sensitivity to CBs leachates. Algal growth inhibition was observed at concentrations as low as 3.38 CB/L for *Dunaliella tertiolecta*, while *Phaeodactylum tricornutum*, the least sensitive species, showed inhibition at 12.4 CB/L. The bacterium *Alivibrio fischeri* exhibited a mean EC50 value for bioluminescence reduction corresponding to 4.47 CB/L. [26] conducted a study that demonstrated an acute toxic effect of the same bacterium at concentrations equivalent to 0.3–2.7 CB/L.

Many literature examples make clear beyond doubt that nicotine released in the aquatic environment can cause many lethal and sub-lethal effects [12,16,27–29]. The mentioned studies proposed a potential genotoxic effect of nicotine due to the bioaccumulation of this emerging pollutant in their tissues.

In our experiment, we could not directly obtain the accumulation of synthetic nicotine in foraminifera. However, in the culture medium, the HPLC evaluation of synthetic nicotine content (N%) after the acute 48 h toxicological tests of April 2021 revealed that the recovery rate of the chemical in the solution ranged from 13% to 23% for the sublethal concentration and from 14% to 16% for the lethal dose (Table 2; Figure 2). This suggests a foraminifera uptake of the remaining synthetic nicotine to roughly between 87% and 77%. Although we cannot exclude the possibility that a small amount of synthetic nicotine may have adhered to the jar's walls containing foraminifera or had been lost during the "washing" procedure after the CTG staining (see method), these high percentages suggest that the cause of foraminiferal death is primarily related to the presence of this alkaloid pollutant. It is worth noting that the recovery rate of synthetic nicotine varies across different foraminiferal species. Notably, *T. agglutinans*, which is one of the most sensitive species, exhibits the potential for significant uptake and demonstrates the lowest recovery rate of synthetic nicotine in the growth medium culture (Figures 1 and 2). The HPLC analysis could not find any trace of cotinine in the growth medium, as also reported in the experiment by [12] that found that cotinine was always below the quantification limit in all experimental conditions, indicating that mussels do not accumulate this chemical released from CBs or do not metabolize nicotine. We suggest that due to their unicellular nature as eukaryotic organisms, foraminifera are also incapable of converting nicotine into its metabolite cotinine. This is attributed to their lack of nicotine acetylcholine receptors (nAChRs) or any similar equivalents [30]. However, we must also consider that the conversion process may require more than 48 h, which is the duration of the experiments conducted on these organisms, therefore hampering its observation.

An important consequence of nicotine pollution in foraminifera is shell decalcification. Some of the evident damages caused by this emerging pollutant include the shell integrity. In fact, the results of the LC50 48 h acute toxicity tests allowed us to hypothesize the involvement of synthetic nicotine as the primary driver for the decalcification of foraminiferal shells (Figure 7). Ref. [18] also reported a notable impact of shell decalcification when the same three species of benthic foraminifera were exposed to CBs' leachates. Foraminifera rely on their shells for structural support and protection. Nicotine accumulation can impact shell formation and structure, leading to abnormalities or the weakening of the shells. This can make them more susceptible to physical damage and dissolution. Specifically, among the examined species, *Rosalina globularis* and *Textularia agglutinans* exhibited the most pronounced decalcification effects, whereas *Quinqueloculina* spp. showed the least susceptibility to this process. This discrepancy may be due to the distinct biomineralization mechanisms characterizing these three species. In fact, *Quinqueloculina* spp. is a miliolid species with an imperforate calcium carbonate shell [31–33]. Its shell lacks pores and consists of continuous mineral crystals, forming a thick, cohesive layer that potentially serves as a more effective barrier against the penetration of the pollutant compared to the shells of *R. globularis* and *T. agglutinans*. *Rosalina globularis* is also a calcareous species, but with a monolamellar and perforate shell structure or hyaline. The test comprises a calcitic lamella with pores traversing the entire shell thickness [34,35]. Due to the presence of channels and the reduced thickness of the shell, it is plausible to assume that synthetic nicotine can be readily absorbed through the foraminiferal shell. *Textularia agglutinans*, being an agglutinated species, solely secretes calcium carbonate cement, which serves as an adhesive for sediment granules and other materials lining the organism's cell. Synthetic nicotine may have a more rapid effect on the decalcification of this cement, leading to the breakdown of the agglutinated shell and an increased uptake by the cell.

In general, the hypothesis is that the shell acts as a barrier, and the susceptibility to different decalcification processes depends on the species' biomineralization pattern. Similarly, the foraminiferal cell's vulnerability to the lethal and sublethal concentrations of synthetic nicotine may vary. Anyhow, it is important to note that the decalcification of the shell does not necessarily equate to the death of the individual.

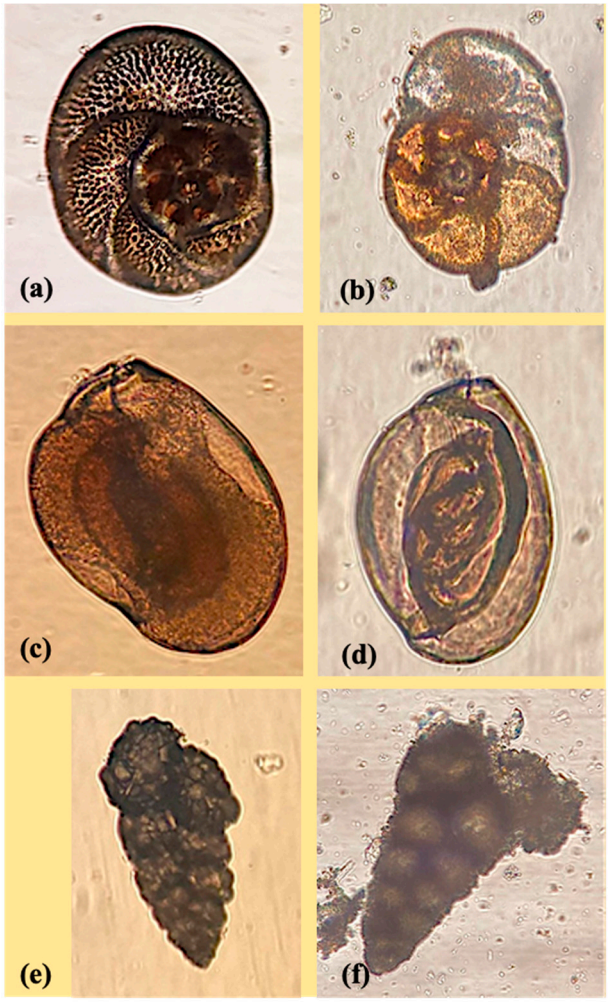


**Figure 7.** Foraminiferal species before (**a**,**c**,**e**) and after (**b**,**d**,**f**) the April 2021 LC50 48 h test observed under the optical microscope. The species are *Rosalina globularis* (**a**,**b**); *Quinqueloculina* spp. (**c**,**d**); and *Textularia agglutinans* (**e**,**f**).

### *4.2. Nicotine and Its Effect on Foraminiferal Macromolecular Composition*

Via the examination of the molecular composition and structure of the shells, the FTIR analyses permitted the discerning of species-specific fingerprints of synthetic nicotine pollution on foraminifera (Figure 3d). By identifying distinct molecular signatures associated with the presence of synthetic nicotine, these analyses have enabled a more precise understanding of how different foraminiferal species respond to this emerging pollutant.

In particular, *R. globularis* and *Quinqueloculina* spp. spectra (Figure 3a,b) show a different distribution of the protein relating to Amide I when compared to the spectrum of the pristine situation. As a matter of fact, in the lethal samples, the decrease in the carbonate broad band at roughly 1410 $cm^{-1}$ makes the Amide I signal clearer; nevertheless, for the samples, it was possible to carry out an in-depth analysis of the protein conformation using the analysis of the second derivatives. To this purpose, the amide I band is the most studied band to determine the conformation of proteins using FTIR [36]. By analyzing the sub-components of this band, it is possible to determine their secondary structure. In both calcareous taxa *R. globularis* (hyaline) and *Quinqueloculina* spp. (miliolid), the exposure to lethal concentrations of synthetic nicotine resulted in noticeable changes in the high-wavenumber region of the amide I band, specifically indicating the accumulation of misfolded protein structures such as beta-sheets and turns (approximately 1660–1690 $cm^{-1}$) (Figures 4d and 5d). Additionally, the main component of the amide I band shifted towards 1640 $cm^{-1}$. The observed changes in protein conformation indicate the presence of cellular

stress and the potential initiation of apoptotic processes within foraminiferal cells [21]. The agglutinated species, *Textularia agglutinans*, behaves similarly to the calcareous species, even when the specimens are exposed to sublethal concentrations of synthetic nicotine during incubation. In Figure 6d, a significant peak at 1640 $cm^{-1}$ can be observed, which is associated with a random coil conformation of proteins (Amide I), indicating disorder in the secondary structure of proteins. Remarkably, [21] also observed is a similar response in the cellular proteins of *R. globularis* when exposed to phthalate (DEHP) in a medium culture for a duration of seven weeks. Additionally, FTIR studies on in situ species, *Rosalina bradyi* and *Textularia bocki*, grown on plastic remains, reveal signals of oxidative stress and protein aggregation. These findings highlight the molecular-level responses of foraminifera to stress, further supporting that these organisms are capable of molecular adaptation, and therefore, are potential good bioindicators.

The cellular response to synthetic nicotine is further evidenced by an increase in lipid content, possibly due to vesicle formation at lethal concentrations for all foraminiferal species (Figure 3, the $CH_X$ stretching at 3000–2800 $cm^{-1}$). In particular, the spectral loading corresponding to PC4 (Figure 4b) displays signals in the lipid regions at 2925 $cm^{-1}$, 2855 $cm^{-1}$, and 1735 $cm^{-1}$, indicating a potential increase in lipid content at lethal concentrations for the most sensitive species, *R. globularis*. In this regard, [12] reported that the exposure to CBs in mussels has been found to modulate lipid metabolism by down-regulating acyl-CoA oxidase, which serves as a signature of lipid peroxidation. Similar impairments in fatty acid metabolism have been observed in various mammalian organs and cell types, with reduced activity of β-oxidation enzymes and increased lipid accumulation following the exposure to cigarette smoke or extracts, as documented by [37,38]. Ref. [39] discovered that polystyrene nanoparticles can be identified within the cytoplasm of the foraminifer *Ammonia parkinsoniana*, leading to the generation of reactive oxygen species (ROS) and an increased accumulation of neutral lipids. Furthermore, Ref. [40] indicated that potential toxicants have been observed to induce cytological modifications in benthic foraminifera of the genus *Ammonia*, including the development of lipid vesicles associated with disturbances in metabolic regulation. These changes in lipid compartments are therefore crucial indicators for assessing adverse conditions, as lipid droplets are believed to sequester contaminants as a protective mechanism for cells [41].

Finally, the literature reports that an increase in lipid concentration also indicates the initiation of the apoptotic process [42]. In further detail, apoptosis is associated with an early accumulation of neutral lipids, mostly in the form of cytoplasmic droplets [43], and the increase in the $CH_2$ signal intensity ratio of fatty acids correlates with the onset of apoptosis [44]. Further, cellular neutral lipids sustain the sequence of blebbing and the formation of apoptotic bodies in cells dying by apoptosis, driving the synthesis of autophagosomal membranes in autophagy [45,46].

### *4.3. Nicotine and Its Effect on Foraminiferal Decalcification*

As described above, the FTIR analyses conclusively confirm the decalcification effect of synthetic nicotine on cultured foraminifera. The accumulation of nicotine in foraminifera can have significant adverse impacts on their shell integrity, leading to the reduction in carbonate production and changes of the shell material properties until the manifestation of malformed shells. In foraminifera, the abnormalities in shell formation are an important indicator of environmental stress and can provide valuable insights into the impact of pollutants and natural disturbances on these organisms. In this regard, the literature extensively documents their shell sensitivity to various anthropogenic pollutants, including heavy metals and hydrocarbons, as well as natural perturbations ([47] and references therein). Like other pollutants, nicotine can interfere with the biological processes involved in shell construction, leading to irregular growth patterns or thinning shells.

At sublethal concentrations, the ratio of carbonates to proteins in *Textularia agglutinans* decreased (Figure 3d). This decrease can be explained by a slight increase in protein signals, along with a significant increase in the bands corresponding to the mineral component

as silicates and carbohydrates (Figure 3c). These findings suggest that the agglutinated species responded by enhancing the production of carbohydrates, potentially representing polysaccharides derived from chitinous or pseudo-chitinous sources that constitute the organic matrix of the foraminiferal shell [48–51]. This response may serve as a defense mechanism against the increased decalcification of calcium carbonate cement while maintaining the stability of the mineral phase of silicates. In contrast, such behavior was not observed in *Rosalina globularis*, where a temporary increase in the carbonates/proteins ratio likely corresponded to a decrease in cellular protein content (Figure 3a).

Nevertheless, both calcareous species, *Rosalina globularis* and *Quinqueloculina* spp., exhibited a response to incubation with the lethal concentration of the pollutant, resulting in a loss of calcium carbonate, as evidenced by the decrease in the carbonates/proteins ratio compared to the control values (Figure 3d).

As marine organisms, such as corals, mollusks, and crustaceans, possess calcium carbonate shells or exoskeletons, this finding strengthens the impact of nicotine in the marine environment as a matter of significant concern. These organisms may therefore be particularly vulnerable to the effects of this emerging pollutant, potentially leading to decalcification. Cases of decalcification are reported in the literature; for instance, *Crassostrea gigas*, exposed to leachate from CBs, exhibited the production of malformed larvae, which is often characterized by extruded and granulated tissues, as well as other types of malformations such as the pre-D larvae stage, a protruded mantle, and indented shells [12]. Also, cigarette consumption was identified as a risk factor for the loss of bone mineral density and osteoporotic fractures in humans [52]. This association is attributed to the detrimental impact of nicotine on osteogenesis, whereby it triggers the activation of nicotinic receptors [53] and binds to calcium channels, leading to a hindrance in calcium accumulation. This disruption subsequently results in the inhibition of bone mineralization. Furthermore, high concentrations of nicotine directly hinder the differentiation of human osteoclasts and promote bone resorption by affecting osteoclast precursors [54].

However, the precise mechanism through which nicotine induces calcium carbonate decalcification in marine organisms remains unknown. The study by [18] on benthic foraminifera revealed that the leachate from CBs had an impact on the vitality and test building mechanism of the same three different benthic species employed in this study. Via the FTIR analysis, the authors hypothesized that foraminiferal death and decalcification processes are not directly linked, but both may be influenced by the pH reduction observed in the CBs' leachate and the toxicity of other dissolved substances, particularly nicotine. These factors can lead to physiological alterations and, in many cases, cellular death.

In contrast, during our experiment, the pH values remained stable at around 8, and synthetic nicotine was the only substance added to the culture medium (i.e., seawater), suggesting that nicotine was the only element responsible for decalcification. When foraminifera are exposed to synthetic nicotine, we hypothesize that the malformations and decalcification processes can be promoted using various mechanisms. In fact, nicotine is known to bind to calcium channels, thereby interfering with the mineralization process in humans by preventing the accumulation of calcium [53]. Similarly, we may speculate that foraminifera are sensitive to the calcium channel blocker represented by the accumulation of nicotine. In this regard, ref. [20] demonstrated that benthic foraminifera, cultured under a range of pharmacological inhibitors targeting calcification-relevant ion channels, exhibited high sensitivity to a calcium channel blocker, demonstrating that the uptake of calcium ions required for calcification in foraminiferal species occurs preferentially via transmembrane transport.

Furthermore, nicotine has been found to affect the activities of specific enzymes involved in calcification processes. For example, it can hinder the catalytic activity of alkaline phosphatase, an enzyme crucial for the hydrolysis of substances that inhibit calcification and the provision of phosphate required for hydroxyapatite crystallization in humans [55]. The exposure to nicotine can cause variation in the activity of different enzymes, further contributing to decalcification in foraminifera. For example, in an experiment on the perforated calcareous species *Amphistegina lessonii*, [56] found that in benthic foraminifera,

intracellular carbonic anhydrase promotes calcification by increasing the rate of $CO_2$ converted to bicarbonate ($HCO_3$). Ref. [57] discovered that, at the site of shell calcification, excess protons from the conversion of $CO_2$ to (bi)carbonate ($CO_3^{2-}$) are transported outside the foraminifera by the V-type $H^+$ ATPase enzyme. Based on these observations, we can hypothesize that nicotine might have entered the membrane channels of foraminifera and interfered with the aforementioned enzymes. Specifically, upon reaching the calcification site, nicotine may have disrupted the outward proton flow generated by the V-type $H^+$ ATPase, leading to an increase in proton concentration within the test. In addition, the protons produced by carbonic anhydrase via the catalysis of $CO_2$ to bicarbonate $HCO_3$ would have contributed to the development of an acidic environment, consequently leading the foraminifera to a weakened shell formation. This stress might have also affected the cellular level, as the presence of nicotine could have significantly altered the foraminiferal metabolism, necessitating the utilization of calcium carbonate from the test as a buffering agent.

Also, nicotine can impact the production of type I collagen via osteoblasts, which are responsible for bone formation in humans [54]. Ref. [51] demonstrated the presence of proteins, such as pre-collagen-P, in the shell organic matrices of the benthic foraminifer *Schlumbergerella floresiana*. Similarly, we can hypothesize that the accumulation of nicotine in the culture medium may affect the production of a collagen-like material present in the organic matrices of foraminiferal shell. A reduction in collagen production could weaken the structural integrity of the shells, making them more susceptible to decalcification.

Finally, we infer that the exposure to anthropogenic nicotine can disrupt calcium homeostasis, impair enzyme activities, and interfere with organic matrix production, all of which may contribute to the decalcification processes observed in foraminifera. Whether individually or in combination, these processes can promote decalcification in foraminifera when exposed to anthropogenic pollutants like nicotine. Consequently, this leads to the loss or deterioration of the calcium carbonate shell, ultimately impacting the health and survival of these organisms.

Considering the scenario just described, the results of this research suggest that foraminifera are sensitive to decalcification caused by the presence of pollutants like nicotine. While the elaborated data pertain to a cultured system, it cannot be excluded that a similar effect may occur in a natural system. In natural environments, in addition to the progressive acidification of water due to climate and anthropogenic change [58], the accumulation of pollutants such as nicotine may accelerate the decalcification process of calcium carbonate. Nicotine accumulation can therefore impact the shell formation and structure, leading to abnormalities or weakening of the shells. This can make them more susceptible to predation, physical damage, or decalcification, and the most important consequence is a reduction in the calcium carbonate availability for the marine ecosystem [9,59,60].

## 5. Conclusions

This study represents the first attempt to evaluate the toxicity of synthetic nicotine on marine-cultured microorganisms. The results demonstrated that both sublethal and lethal concentrations of synthetic nicotine have an impact on the viability, shell-building mechanism, and cell macromolecular composition of three studied foraminiferal species: the perforated calcareous *Rosalina globularis*, the imperforate calcareous (miliolid) *Quinqueloculina* spp., and the agglutinated foraminifer *Textularia agglutinans*.

The two LC50 48 h tests revealed that synthetic nicotine is acutely toxic to all three foraminiferal species, with each exhibiting a specific response related to the type of shell biomineralization. The HPLC analyses confirmed that foraminifera absorbed a significant amount of synthetic nicotine but were unable to convert it to cotinine within 48 h. Furthermore, the FTIR analyses demonstrated that synthetic nicotine promotes shell decalcification and alters the composition of cytoplasmic macromolecules (such as lipids and proteins) in foraminifera exposed to this emerging pollutant.

The comparison of our results with the ecotoxicological studies conducted on other marine organisms allowed us to establish the importance of benthic foraminifera as important bioindicators for CBs' pollution in the sea. Overall, this research contributes to demonstrating that foraminifera can serve as reliable indicators of CBs' pollution in the sea, with nicotine emerging as a pollutant capable of causing cellular stress and shell damage in these organisms.

Foraminifera play crucial roles in marine ecosystems as both food sources for other organisms and indicators of environmental conditions. The accumulation of nicotine can disrupt their physiology and behavior, potentially interfering with the ecological interactions they engage in with other marine organisms. Changes in the abundance or health of foraminiferal populations resulting from nicotine accumulation can have repercussions on the overall composition of marine communities. This, in turn, can lead to cascading effects on other organisms that rely on foraminifera as a source of food or habitat. In summary, the accumulation of nicotine in foraminifera can have significant adverse impacts on their biology, shell integrity, ecological functions, and the broader marine ecosystems they inhabit.

**Author Contributions:** Conceptualization, A.S., F.C., A.A. and G.M.; methodology, A.S., F.C., E.C., G.B., A.A. and G.M.; validation, A.S.; formal analysis, A.S., F.C., E.C., G.B., A.A. and G.M.; investigation, A.S., F.C. and G.B.; resources, G.B. and A.A.; data curation, A.S., F.C., G.B. and A.A.; writing—original draft preparation, A.S., F.C. and G.B.; writing—review and editing, A.S., G.B., C.B., D.M., G.D.G. and A.N.; visualization, A.S., F.C. and G.B.; supervision, A.S. and A.N. All authors have read and agreed to the published version of the manuscript.

**Funding:** This research received no external funding.

**Institutional Review Board Statement:** Not applicable.

**Informed Consent Statement:** Not applicable.

**Data Availability Statement:** Not applicable.

**Acknowledgments:** The authors acknowledge Lucrezia Spaziani for her collaboration in sampling, picking, and analyzing the sediment samples. The authors wish to acknowledge ICare grant (PRIN_2020_2020EEMH5R_Sabbatini). The authors acknowledge the CERIC-ERIC Consortium for the access to experimental facilities with proposal number 20222153 and financial support.

**Conflicts of Interest:** The authors declare no conflict of interest.

## Appendix A

Details on HPLC analytical methods and procedures

### High Performance Liquid Chromatography analysis (HPLC)

The chromatography apparatus was a Young Lin Instruments chromatograph consisting of a YL9111 binary pump, a YL9160 PDA detector, and an HTA-MT300L-E auto-sampler (HTA s.r.l., Brescia, Italy) operated via its integrated software and connected to a C-18 reverse phase column, Synegi RP 4 μm, 80 A, 250 mm × 4.6 mm i.d. (Phenomenex Inc., Torrance, CA, USA). The column was equilibrated with 0.050 M of $KH_2PO_4$ buffer, adjusted to pH 6.1 via KOH, containing 5 mM of Heptane-1-Sulfonic Acid sodium salt as the ion pair agent, at a 1.0 mL/min flow rate (buffer A), and washed with 40% methanol in the same buffer (buffer B) in between samples. Chromatograms were acquired via a diode array detector and integrated at a 260 nm wavelength using the nicotine and cotinine standards for quantization. Compounds were identified using the retention time and UV spectrum correspondence.

Three standard solutions were prepared, containing nicotine salt, free base nicotine, and cotinine, respectively:

- Nicotine salt (nicotine hemisulfate salt, 35% *w/v* in $H_2O$, Sigma-Aldrich, St. Louis, MO, USA) standard was made with 20 mM in buffer A.

- Free base nicotine (≥99% (TLC), liquid, Sigma-Aldrich, St. Louis, MO, USA) base standard was made with 20 mM in buffer A.
- Cotinine (≥98%, Sigma-Aldrich, St. Louis, MO, USA) standard was made with 20 nM in buffer A.

Before loading all samples, the HPLC parameters for the analysis were set as follows:

- Gradient curve
- 40% methanol
- T = 45.9 °C

The samples were loaded onto the HPLC, each with a volume of 200 µL, by first placing the control (with MilliQ water only) and then the three standards (in order: nicotine salt, pure nicotine, and cotinine). As previously set up, the instrument analyzed an aliquot of 30 µL for each sample and the VWD PDA detector was set at 260 nm, enabling the wavelength at which nicotine and cotinine could reach the maximum absorbance.

After identifying the absorbance peaks over time for the three standards, a solution defined as Mix were prepared:

- Mix 1 = nicotine salt (5 µL) + cotinine (5 µL) + mobile phase B with 18% methanol (990 µL)
- Mix 2 = nicotine salt (5 µL) + cotinine (5 µL) + mobile phase B with 18% methanol (990 µL)
- Mix 3 = nicotine salt (5 µL) + cotinine (5 µL) + pure nicotine (5 µL) + mobile phase B with 18% methanol (958 µL).

To each mix, a concentration of 3 mol of KCl was added to bring forward the peaks.

This Mix was analyzed to understand if the instrument was able to detect the single standard peak within the Mix solution maintaining the same characteristics (absorbance and retention time).

In order, after the control, the experimental samples of the LC50 48 h test were loaded onto the HPLC, which were previously processed using the following steps:

(1) Lyophilization.
(2) Mixing for 10 min, adding to each sample 4 mL of mobile phase (2 mL of phase A and 2 mL of phase B) with 20% methanol.
(3) Sonication for 1 min, keeping the samples on ice.
(4) Centrifuging for 10 min (at 22,000 rpm) and supernatant was utilized for HPLC analysis.

They were then processed to estimate the synthetic nicotine recovery rate expressed in percentages (N%). These data were calculated from chromatograms which describe the absorbance (mAu) over time (min). In particular, the selected areas subtended from the curve of each chromatogram were used to calculate the value; in fact, the measured area is normally proportional to the quantity or concentration of the eluted substance (in this case, synthetic nicotine).

**Synthetic nicotine determination**

To determine the synthetic nicotine recovery rate for each sample, the initial (µmol) and total (µmol) synthetic nicotine concentrations were calculated as follows:

$$\mu mol = (\mu L \times d \times 35/100)/PM \times 1000$$

where µL is the initial synthetic nicotine used for the experiment; d is the nicotine salt solution density; and 35/100 is the nicotine salt solution concentration.

$$\mu molt = (Nc\ (nmol))/(30\ \mu L \times 4000/1000)$$

where Nc is the synthetic nicotine concentration; 30 µL is the aliquot analyzed using the instrument; and 4 mL is the volume of the mobile phase added to each sample.

The synthetic nicotine concentration expressed in nmol is calculated using the standards values (areas and concentration) as:

$$\text{nmols:areas} = \text{X:area}$$

where nmols is the initial concentration of nicotine used to set up the standards; area is the chromatogram area of the nicotine standard; and area is the chromatogram area of the sample.

$$N\% = (\mu\text{molt})/(\mu\text{moli}) \times 100$$

## Appendix B

The synthetic nicotine recovery rates (N%) for each nicotine-solution sample.

| Foraminiferal Species | Replicates | mL Nicotine ($HSO_4$-) | Area (mAu) | nmoles | Initial Mmoles of Synthetic Nicotine in Solution Samples | Final Mmoles of Synthetic Nicotine in Solution Samples | Nicotine Recovery Rate (%) |
|---|---|---|---|---|---|---|---|
| *Rosalina globularis* | Control | 0 | 0 | 0 | 0 | 0 | 0 |
| | R1—sublethal | 2.24 | 641.041 | 2.93 | 2.1 | 0.4 | **18.3** |
| | R1—sublethal | 2.24 | 1111.953 | 5.08 | 2.1 | 0.7 | **31.8** |
| | R1—sublethal | 2.24 | 595.455 | 2.72 | 2.1 | 0.4 | **17.0** |
| | R1—$LC_{50}$ | 4.2 | 1030.853 | 4.71 | 4.0 | 0.6 | **15.7** |
| | R1—$LC_{50}$ | 4.2 | 902.317 | 4.12 | 4.0 | 0.5 | **13.7** |
| | R1—$LC_{50}$ | 4.2 | 1269.829 | 5.8 | 4.0 | 0.8 | **19.3** |
| *Quinqueloculina* spp. | Control | 0 | 0 | 0 | 0 | 0 | 0 |
| | R1—sublethal | 4.46 | 901.549 | 4.12 | 4.2 | 0.5 | **12.9** |
| | R1—sublethal | 4.46 | 945.711 | 4.32 | 4.2 | 0.6 | **13.6** |
| | R1—sublethal | 4.46 | 1139.925 | 5.21 | 4.2 | 0.7 | **16.4** |
| | R1—$LC_{50}$ | 16.0 | 3509.625 | 16.04 | 15.2 | 2.1 | **14.0** |
| | R1—$LC_{50}$ | 16.0 | 3906.988 | 17.86 | 15.2 | 2.4 | **15.6** |
| | R1—$LC_{50}$ | 16.0 | 3535.302 | 16.16 | 15.2 | 2.2 | **14.1** |
| *Textularia agglutinans* | Control | 0 | 0 | 0 | 0 | 0 | 0 |
| | R1—sublethal | 4.46 | 743.195 | 3.40 | 4.2 | 0.5 | **10.7** |
| | R1—sublethal | 4.46 | 1107.947 | 5.06 | 4.2 | 0.7 | **15.9** |
| | R1—sublethal | 4.46 | 1058.257 | 4.84 | 4.2 | 0.6 | **15.2** |
| | R1—$LC_{50}$ | 12.5 | 2990.652 | 13.67 | 11.9 | 1.8 | **15.3** |
| | R1—$LC_{50}$ | 12.5 | 2746.864 | 12.56 | 11.9 | 1.7 | **14.1** |
| | R1—$LC_{50}$ | 12.5 | 2658.851 | 12.15 | 11.9 | 1.6 | **13.6** |

## References


1. Cau, A.; Avio, C.G.; Dessì, C.; Moccia, D.; Pusceddu, A.; Regoli, F.; Cannas, R.; Follesa, M.C. Benthic Crustacean Digestion Can Modulate the Environmental Fate of Microplastics in the Deep Sea. *Environ. Sci. Technol.* **2020**, *54*, 4886–4892. [CrossRef] [PubMed]
2. Asensio-Montesinos, F.; Anfuso, G.; Williams, A.T. Beach Litter Distribution along the Western Mediterranean Coast of Spain. *Mar. Pollut. Bull.* **2019**, *141*, 119–126. [CrossRef] [PubMed]
3. Becherucci, M.E.; Rosenthal, A.F.; Pon, J.P.S. Marine Debris in Beaches of the Southwestern Atlantic: An Assessment of Their Abundance and Mass at Different Spatial Scales in Northern Coastal Argentina. *Mar. Pollut. Bull.* **2017**, *119*, 299–306. [CrossRef] [PubMed]
4. Wilson, S.P.; Verlis, K.M. The Ugly Face of Tourism: Marine Debris Pollution Linked to Visitation in the Southern Great Barrier Reef, Australia. *Mar. Pollut. Bull.* **2017**, *117*, 239–246. [CrossRef] [PubMed]
5. Araújo, M.C.B.; Costa, M.F. A Critical Review of the Issue of Cigarette Butt Pollution in Coastal Environments. *Environ. Res.* **2019**, *172*, 137–149. [CrossRef]
6. Li, L.; Yang, D.C.; Chen, C.-H. Metabolic Reprogramming: A Driver of Cigarette Smoke-Induced Inflammatory Lung Diseases. *Free Radic. Biol. Med.* **2021**, *163*, 392–401. [CrossRef]

7. Torkashvand, J.; Farzadkia, M.; Sobhi, H.R.; Esrafili, A. Littered Cigarette Butt as a Well-Known Hazardous Waste: A Comprehensive Systematic Review. *J. Hazard. Mater.* **2020**, *383*, 121242. [CrossRef]
8. Ockene, I.S.; Miller, N.H. Cigarette Smoking, Cardiovascular Disease, and Stroke: A Statement for Healthcare Professionals from the American Heart Association. *Circulation* **1997**, *96*, 3243–3247. [CrossRef]
9. Dobaradaran, S.; Soleimani, F.; Akhbarizadeh, R.; Schmidt, T.C.; Marzban, M.; BasirianJahromi, R. Environmental Fate of Cigarette Butts and Their Toxicity in Aquatic Organisms: A Comprehensive Systematic Review. *Environ. Res.* **2021**, *195*, 110881. [CrossRef]
10. Rebischung, F.; Chabot, L.; Biaudet, H.; Pandard, P. Cigarette Butts: A Small but Hazardous Waste, According to European Regulation. *Waste Manag.* **2018**, *82*, 9–14. [CrossRef]
11. Bonanomi, G.; Maisto, G.; De Marco, A.; Cesarano, G.; Zotti, M.; Mazzei, P.; Libralato, G.; Staropoli, A.; Siciliano, A.; De Filippis, F. The Fate of Cigarette Butts in Different Environments: Decay Rate, Chemical Changes and Ecotoxicity Revealed by a 5-Years Decomposition Experiment. *Environ. Pollut.* **2020**, *261*, 114108. [CrossRef]
12. Lucia, G.; Giuliani, M.E.; d'Errico, G.; Booms, E.; Benedetti, M.; Di Carlo, M.; Fattorini, D.; Gorbi, S.; Regoli, F. Toxicological Effects of Cigarette Butts for Marine Organisms. *Environ. Int.* **2023**, *171*, 107733. [CrossRef]
13. Quéméneur, M.; Chifflet, S.; Akrout, F.; Bellaaj-Zouari, A.; Belhassen, M. Impact of Cigarette Butts on Microbial Diversity and Dissolved Trace Metals in Coastal Marine Sediment. *Estuar. Coast. Shelf Sci.* **2020**, *240*, 106785. [CrossRef]
14. Green, D.S.; Kregting, L.; Boots, B. Effects of Cigarette Butts on Marine Keystone Species (*Ulva lactuca* L. and *Mytilus edulis* L.) and Sediment Microphytobenthos. *Mar. Pollut. Bull.* **2021**, *165*, 112152. [CrossRef]
15. Booth, D.J.; Gribben, P.; Parkinson, K. Impact of Cigarette Butt Leachate on Tidepool Snails. *Mar. Pollut. Bull.* **2015**, *95*, 362–364. [CrossRef] [PubMed]
16. Wright, S.L.; Rowe, D.; Reid, M.J.; Thomas, K.V.; Galloway, T.S. Bioaccumulation and Biological Effects of Cigarette Litter in Marine Worms. *Sci. Rep.* **2015**, *5*, 14119. [CrossRef] [PubMed]
17. Soleimani, F.; Dobaradaran, S.; Vazirizadeh, A.; Mohebbi, G.; Ramavandi, B.; De-la-Torre, G.E.; Nabipour, I.; Schmidt, T.C.; Novotny, T.E.; Maryamabadi, A. Chemical Contents and Toxicity of Cigarette Butts Leachates in Aquatic Environment: A Case Study from the Persian Gulf Region. *Chemosphere* **2023**, *311*, 137049. [CrossRef]
18. Caridi, F.; Sabbatini, A.; Birarda, G.; Costanzi, E.; De Giudici, G.; Galeazzi, R.; Medas, D.; Mobbili, G.; Ricciutelli, M.; Ruello, M.L. Cigarette Butts, a Threat for Marine Environments: Lessons from Benthic Foraminifera (Protista). *Mar. Environ. Res.* **2020**, *162*, 105150. [CrossRef]
19. Matta, S.G.; Balfour, D.J.; Benowitz, N.L.; Boyd, R.T.; Buccafusco, J.J.; Caggiula, A.R.; Craig, C.R.; Collins, A.C.; Damaj, M.I.; Donny, E.C. Guidelines on Nicotine Dose Selection for in Vivo Research. *Psychopharmacology* **2007**, *190*, 269–319. [CrossRef] [PubMed]
20. Keul, N.; Schmidt, S. Calcification in Foraminifera Largely Supported by Ion Channels-Biomineralization Pathways and Their Effect on Trace Elemental Composition. In *AGU Fall Meeting Abstracts*; American Geophysical Union: Washington, DC, USA, 2018; Volume 2018, p. PP43A-02.
21. Birarda, G.; Buosi, C.; Caridi, F.; Casu, M.A.; De Giudici, G.; Di Bella, L.; Medas, D.; Meneghini, C.; Pierdomenico, M.; Sabbatini, A. Plastics, (Bio)Polymers and Their Apparent Biogeochemical Cycle: An Infrared Spectroscopy Study on Foraminifera. *Environ. Pollut.* **2021**, *279*, 116912. [CrossRef] [PubMed]
22. Murray, J.W. *Ecology and Applications of Benthic Foraminifera*; Cambridge University Press: Cambridge, UK, 2006.
23. Ross, B.J.; Hallock, P. Challenges in Using CellTracker Green on Foraminifers That Host Algal Endosymbionts. *PeerJ* **2018**, *6*, e5304. [CrossRef] [PubMed]
24. Bernhard, J.M.; Ostermann, D.R.; Williams, D.S.; Blanks, J.K. Comparison of Two Methods to Identify Live Benthic Foraminifera: A Test between Rose Bengal and CellTracker Green with Implications for Stable Isotope Paleoreconstructions. *Paleoceanography* **2006**, *21*, PA4210. [CrossRef]
25. Ross, B. *Responses to Chemical Exposure by Foraminifera: Distinguishing Dormancy from Mortality*; University of South Florida: Tampa, FL, USA, 2012.
26. Massadeh, A.M.; Gharaibeh, A.A.; Omari, K.W. A single-step extraction method for the determination of nicotine and cotinine in Jordanian smokers' blood and urine samples by RP-HPLC and GC–MS. *J. Chromatogr. Sci.* **2009**, *47*, 170–177.
27. Konar, S.K. Histopathological Effects of the Insecticides, Heptachlor and Nicotine, on the Gills of the Catfish, Heteropneustes Fossilis. *Jpn. J. Ichthyol.* **1969**, *15*, 156–159.
28. Konar, S.K. Toxicity of Nicotine to Aquatic Life. *Indian J. Fish. Ernakulam* **1977**, *24*, 124–128.
29. Chang, P.-H.; Chiang, C.-H.; Ho, W.-C.; Wu, P.-Z.; Tsai, J.-S.; Guo, F.-R. Combination Therapy of Varenicline with Nicotine Replacement Therapy Is Better than Varenicline Alone: A Systematic Review and Meta-Analysis of Randomized Controlled Trials. *BMC Public. Health* **2015**, *15*, 1–8. [CrossRef]
30. Cecchini, M.; Changeux, J.-P. The Nicotinic Acetylcholine Receptor and Its Prokaryotic Homologues: Structure, Conformational Transitions & Allosteric Modulation. *Neuropharmacology* **2015**, *96*, 137–149.
31. de Nooijer, L.J.; Toyofuku, T.; Oguri, K.; Nomaki, H.; Kitazato, H. Intracellular PH Distribution in Foraminifera Determined by the Fluorescent Probe HPTS. *Limnol. Oceanogr. Methods* **2008**, *6*, 610–618. [CrossRef]
32. De Nooijer, L.J.; Toyofuku, T.; Kitazato, H. Foraminifera Promote Calcification by Elevating Their Intracellular PH. *Proc. Natl. Acad. Sci. USA* **2009**, *106*, 15374–15378. [CrossRef]

33. Zamora-Duran, M.A.; Aronson, R.B.; Leichter, J.J.; Flannery, J.A.; Richey, J.N.; Toth, L.T. Imprint of Regional Oceanography on Foraminifera of Eastern Pacific Coral Reefs. *J. Foraminifer. Res.* **2020**, *50*, 279–290. [CrossRef]
34. Erez, J. The Source of Ions for Biomineralization in Foraminifera and Their Implications for Paleoceanographic Proxies. *Rev. Mineral. Geochem.* **2003**, *54*, 115–149. [CrossRef]
35. de Nooijer, L.J.; Spero, H.J.; Erez, J.; Bijma, J.; Reichart, G.-J. Biomineralization in Perforate Foraminifera. *Earth-Sci. Rev.* **2014**, *135*, 48–58. [CrossRef]
36. Barth, A. Infrared Spectroscopy of Proteins. *Biochim. Biophys. Acta (BBA)-Bioenerg.* **2007**, *1767*, 1073–1101. [CrossRef] [PubMed]
37. Gong, J.; Zhao, H.; Liu, T.; Li, L.; Cheng, E.; Zhi, S.; Kong, L.; Yao, H.-W.; Li, J. Cigarette Smoke Reduces Fatty Acid Catabolism, Leading to Apoptosis in Lung Endothelial Cells: Implication for Pathogenesis of COPD. *Front. Pharmacol.* **2019**, *10*, 941. [CrossRef] [PubMed]
38. Gupta, R.; Lin, Y.; Luna, K.; Logue, A.; Yoon, A.J.; Haptonstall, K.P.; Moheimani, R.; Choroomi, Y.; Nguyen, K.; Tran, E. Electronic and Tobacco Cigarettes Alter Polyunsaturated Fatty Acids and Oxidative Biomarkers. *Circ. Res.* **2021**, *129*, 514–526. [CrossRef] [PubMed]
39. Ciacci, C.; Grimmelpont, M.V.; Corsi, I.; Bergami, E.; Curzi, D.; Burini, D.; Bouchet, V.M.; Ambrogini, P.; Gobbi, P.; Ujiié, Y. Nanoparticle-Biological Interactions in a Marine Benthic Foraminifer. *Sci. Rep.* **2019**, *9*, 19441. [CrossRef] [PubMed]
40. Le Cadre, V.; Debenay, J.-P. Morphological and Cytological Responses of Ammonia (Foraminifera) to Copper Contamination: Implication for the Use of Foraminifera as Bioindicators of Pollution. *Environ. Pollut.* **2006**, *143*, 304–317. [CrossRef]
41. Murphy Jr, G.; Rouse, R.L.; Polk, W.W.; Henk, W.G.; Barker, S.A.; Boudreaux, M.J.; Floyd, Z.E.; Penn, A.L. Combustion-Derived Hydrocarbons Localize to Lipid Droplets in Respiratory Cells. *Am. J. Respir. Cell Mol. Biol.* **2008**, *38*, 532–540. [CrossRef]
42. Boren, J.; Brindle, K.M. Apoptosis-Induced Mitochondrial Dysfunction Causes Cytoplasmic Lipid Droplet Formation. *Cell Death Differ.* **2012**, *19*, 1561–1570. [CrossRef]
43. Al-Saffar, N.M.S.; Titley, J.C.; Robertson, D.; Clarke, P.A.; Jackson, L.E.; Leach, M.O.; Ronen, S.M. Apoptosis Is Associated with Triacylglycerol Accumulation in Jurkat T-Cells. *Br. J. Cancer* **2002**, *86*, 963–970. [CrossRef]
44. Schmitz, J.E.; Kettunen, M.I.; Hu, D.-E.; Brindle, K.M. 1H MRS-Visible Lipids Accumulate during Apoptosis of Lymphoma Cells in Vitro and in Vivo. *Magn. Reson. Med. Off. J. Int. Soc. Magn. Reson. Med.* **2005**, *54*, 43–50. [CrossRef]
45. Cristea, I.M.; Degli Esposti, M. Membrane Lipids and Cell Death: An Overview. *Chem. Phys. Lipids* **2004**, *129*, 133–160. [CrossRef] [PubMed]
46. Crimi, M.; Degli Esposti, M. Apoptosis-Induced Changes in Mitochondrial Lipids. *Biochim. Biophys. Acta (BBA)-Mol. Cell Res.* **2011**, *1813*, 551–557. [CrossRef] [PubMed]
47. Pati, P.; Patra, P.K. Benthic foraminiferal responses to coastal pollution: A review. *Int. J. Geol.* **2012**, *2*, 42–56.
48. Loeblich, A.R.; Tappan, H. Foraminiferal Classification and Evolution. *Geol. Soc. India* **1964**, *5*, 5–40.
49. Traverse, A. *Paleopalynology*; Springer Science & Business Media: Berlin/Heidelberg, Germany, 2007; Volume 28.
50. Banner, F.T. Test Structure, Organic Skeleton and Extrathalamous Cytoplasm of Ammonia Brunnich. *J. Foraminifer. Res.* **1973**, *3*, 49–69. [CrossRef]
51. Sabbatini, A.; Morigi, C.; Nardelli, M.P.; Negri, A. Foraminifera. In *The Mediterranean Sea*; Goffredo, S., Dubinsky, Z., Eds.; Springer Netherlands: Dordrecht, The Netherland, 2014; pp. 237–256. ISBN 978-94-007-6703-4.
52. Krall, E.A.; Dawson-Hughes, B. Smoking Increases Bone Loss and Decreases Intestinal Calcium Absorption. *J. Bone Min. Res.* **1999**, *14*, 215–220. [CrossRef]
53. Tanaka, H.; Tanabe, N.; Kawato, T.; Nakai, K.; Kariya, T.; Matsumoto, S.; Zhao, N.; Motohashi, M.; Maeno, M. Nicotine Affects Bone Resorption and Suppresses the Expression of Cathepsin K, MMP-9 and Vacuolar-Type $H^+$-ATPase D2 and Actin Organization in Osteoclasts. *PLoS ONE* **2013**, *8*, e59402. [CrossRef]
54. Costa-Rodrigues, J.; Rocha, I.; Fernandes, M.H. Complex Osteoclastogenic Inductive Effects of Nicotine over Hydroxyapatite. *J. Cell Physiol.* **2018**, *233*, 1029–1040. [CrossRef]
55. Tanaka, H.; Tanabe, N.; Suzuki, N.; Shoji, M.; Torigoe, H.; Sugaya, A.; Motohashi, M.; Maeno, M. Nicotine Affects Mineralized Nodule Formation by the Human Osteosarcoma Cell Line Saos-2. *Life Sci.* **2005**, *77*, 2273–2284. [CrossRef]
56. De Goeyse, S.; Webb, A.E.; Reichart, G.-J.; De Nooijer, L.J. Carbonic Anhydrase Is Involved in Calcification by the Benthic Foraminifer *Amphistegina lessonii*. *Biogeosciences* **2021**, *18*, 393–401. [CrossRef]
57. Toyofuku, T.; Matsuo, M.Y.; De Nooijer, L.J.; Nagai, Y.; Kawada, S.; Fujita, K.; Reichart, G.-J.; Nomaki, H.; Tsuchiya, M.; Sakaguchi, H.; et al. Proton Pumping Accompanies Calcification in Foraminifera. *Nat. Commun.* **2017**, *8*, 14145. [CrossRef] [PubMed]
58. Zeebe, R.E.; Ridgwell, A.; Zachos, J.C. Anthropogenic Carbon Release Rate Unprecedented during the Past 66 Million Years. *Nat. Geosci.* **2016**, *9*, 325–329. [CrossRef]
59. Prazeres, M.; Uthicke, S.; Pandolfi, J.M. Ocean Acidification Induces Biochemical and Morphological Changes in the Calcification Process of Large Benthic Foraminifera. *Proc. R. Soc. B* **2015**, *282*, 20142782. [CrossRef]
60. Byrne, M.; Fitzer, S. The Impact of Environmental Acidification on the Microstructure and Mechanical Integrity of Marine Invertebrate Skeletons. *Conserv. Physiol.* **2019**, *7*, coz062. [CrossRef]